Indian Journal of Chemistry
Vol. 56A, March 2017, pp. 270-277

Papers

Photocatalytic and DC conductivity studies of proton exchanged $KAl_{0.33}W_{1.67}O_6$ and its application in Pb^{2+} removal

M Srinivas, G Ravi, P Vijaya Kumar, CH Sudhakar Reddy, Sreenu K, Ravinder Guje & M Vithal*

Department of Chemistry, Osmania University, Hyderabad 500 007, Telangana
Email: mugavithal@gmail.com

Received 28 November 2016; revised and accepted 26 February 2017

The proton exchanged metal oxide of composition $HAl_{0.33}Te_{1.67}O_6$ (HAW) is synthesized by ion exchange method at room temperature and characterized by X-ray diffraction, scanning electron microscopy, energy dispersive spectroscopy, Fourier transform infrared spectroscopy, Raman spectroscopy and UV-vis diffuse reflectance spectroscopy. Presence of water content in the HAW has been examined by thermogravimetric analysis. Conductivity and photocatalytic properties of HAW are compared with those of its parent $KAl_{0.33}W_{1.67}O_6$ (KAW). $HAl_{0.33}W_{1.67}O_6$ shows higher conductivity and photocatalytic activity for the degradation of methyl blue and Rhodamine B under visible light irradiation. Participation of hydroxyl radicals in the photocatalytic dye degradation has been investigated by photoluminescence studies using terephthalic acid as probe. The removal of Pb^{2+} from an aqueous solution of $Pb(NO_3)_2$ using pristine $KAl_{0.33}W_{1.67}O_6$ is also reported.

Keywords: Photocatalytic activity, Powder X-ray diffraction, Bandgap energy, Conductivity, Lead

Ion conducting oxides have remarkable technological significance, particularly for their applications in sensors, fuel cells and steam electrolysis cells. Different types of three-dimensional skeletal structures are known to facilitate fast ion conduction[1,2]. Among these structures, defect pyrochlore materials offer interesting possibilities to act as fast-ion conductors due to its structural and compositional flexibility. The general formula of defect pyrochlore is AB_2O_6 and its structure is built up of corner sharing BO_6 octahedra creating networks of hexagonal B_2O_6 tunnels. The "A" ions are present in these tunnels and can move freely and are responsible for ionic conduction. Further, defect pyrochlore oxides having smaller cation such as H^+ show relatively high ionic conductivity due to its the high mobility through the interconnecting three dimensional channels. However, reports on proton conductivity of defect pyrochlores are scanty[3-9].

$KAl_{0.33}W_{1.67}O_6$ (KAW) belongs to defect pyrochlore family and its general formula is $AB_{0.33}B'_{1.67}O_6$. The potassium ions are located in $(Al/W)_2O_6$ tunnels and can be substituted by mono, di or trivalent ions and this substitution also leads to incorporation of neutral solvent molecules into the lattice. Recently, we have studied the structural and compositional flexibility of KAW by exchanging K^+ with Sn^{2+}, Sm^{3+} and Eu^{3+} for possible applications in energy and environmental fields[10-12]. Generally, the ion exchange method affords an alternative to high temperature synthetic procedures and is widely used in both industrial and academic environments. A few studies on ion exchange properties of materials with defect pyrochlore structure have been reported[2,13,14]. These studies have shown that the defect pyrochlore lattice is suitable for the removal of toxic metal ions from industrial waste water and nuclear effluents[11,13-17]. The removal of these toxic metal ions from aqueous systems is vital for the safety of the public health and environment. In view of these reports, an attempt is made to investigate the conductivity and photocatalytic activity of proton exchanged KAW along with removal of toxic Pb^{2+} by KAW from aqueous solution of $Pb(NO_3)_2$.

Materials and Methods

Preparation of H^+ doped $KAl_{0.33}W_{1.67}O_6$

$KAl_{0.33}W_{1.67}O_6$ (KAW) was prepared by gel burning method[10] By the following procedure: stoichiometric amounts of KNO_3 and $Al(NO_3)_3$ were first dissolved in doubly distilled water separately and labeled as "solution A" and "solution B",

respectively. Tungsten (W) metal powder was dissolved in H_2O_2 solution in an ice bath. It took about 6 h for complete dissolution of tungsten powder. The resultant clear solution was labeled as "solution C". Solutions A and B were slowly added to solution C in an ice bath. The chelating agent, citric acid, was then added. The molar ratio of citric acid to metal ions was 2:1. The pH of the resultant metal citrate solution was adjusted to 6-7 by adding dilute ammonia solution dropwise. The solution was then slowly evaporated on a water bath until a viscous liquid was obtained. At this stage, the gelating reagent, ethylene glycol, was added to the solution. The molar ratio of citric acid to ethylene glycol was 1.0:1.2. This mixture was heated on a hot plate at 100 °C for 2-3 hours with constant stirring. The temperature was increased to 160-180 °C at the onset of solidification. The ensuing solid porous mass was ground in an agate mortar using spectral grade acetone. The resultant black powder was heated in a muffle furnace at 700 °C for 5 h.

The proton exchanged KAW was prepared by ion exchange method. KAW (1 g) was added to 100 mL of 5 *M* concentrated hydrochloric acid at room temperature with constant stirring for 48 h. The resulting material was filtered and dried and designated as HAW. Experiments to substantiate the exchange of K^+ by H^+ were also carried out. The filtrate was evaporated slowly and the resultant product (say byproduct) was dried and subjected to powder XRD.

Ion exchange experiment for the removal of Pb^{2+} in aqueous solution

Han *et al*. have reported an ion exchange method for the removal of Pb^{2+} from an aqueous solution of $Pb(NO_3)_2$ using defect pyrochlore, $KNbWO_6$ H_2O[14]. In the present investigation, attempts are made to remove the toxic Pb^{2+} ion in an aqueous solution of $Pb(NO_3)_2$ with $KAl_{0.33}W_{1.67}O_6$. The ion exchange procedure is as follows: About 0.5 g of $KAl_{0.33}W_{1.67}O_6$ is added to 100 mL of 0.011 *M* solution (natural pH = 3) of $Pb(NO_3)_2$ and stirred for 24 h at room temperature. The resultant product (PbKAW) was washed with doubly distilled water several times and dried. The concentration of un-exchanged Pb^{2+} in the filtrate was determined by atomic absorption spectroscopy (AAS) using a Perkin–Elmer A Analyst–700 instrument.

Characterization

The room temperature powder X-ray diffractograms were recorded using Rigaku miniplex powder X-ray diffractometer (Cu-Kα, λ = 1.5406 Å) in the 2θ range 10 - 80° for phase confirmation. Infrared spectra were recorded in the form of KBr pellets in the wave number range 4000–400 cm^{-1} using Jasco IR-5300 spectrometer. Thermogravimetric analysis (TGA) was performed using Shimadzu differential thermal analyzer (DTG-60H) with a heating rate of 15 °C min^{-1}. Raman spectra were recorded using a 632.81 nm line from a He-Ne laser and the scattered light was analyzed using HORIBA JOBIN YVON HR800. The laser was focused on a spot of ~3 μm and a 10X lens was used for the collection of back scattered Raman signal. The room temperature ^1H and ^{27}Al solid-state MAS NMR spectra were recorded with a Bruker MSL-300 MHz solid-state high- resolution spectrometer operating at 121.49 MHz with a 10 kHz spinning speed. SEM images of all the materials were recorded on the HITACHI SU-1500 variable pressure scanning electron microscope (VP-SEM). JASCO V650 UV-vis spectrophotometer was used for UV-vis diffuse reflectance spectral (DRS) measurements in the range 200 – 800 nm. $BaSO_4$ was used as the reflectance standard.

Photocatalytic activity

The photocatalytic activity of HAW was evaluated by photodegradation of methyl blue (MB) and Rhodamine B (RhB) under visible light irradiation using HEBER visible annular type photo reactor equipped with a 300 watts W lamp (wavelength range: 380-840 nm). In a typical process, 50 mL of aqueous MB (or RhB) solution with an initial concentration of $1x10^{-5}$ *M* and 50 mg of catalyst are taken in a cylindrical-shaped glass reactor at room temperature in air. The suspension was stirred in the dark for 60 min to establish adsorption - desorption equilibrium before the irradiation. At regular time intervals of 30 min, about 2–3 mL of the solution was collected and centrifuged to remove the catalyst particles. The change in the concentration of collected solution of MB (or RhB) was obtained by recording the absorbance at 664 (or 554) nm using Jasco V650 UV-vis spectrophotometer.

The formation of $OH^{\bullet}$ radicals during photocatalysis under visible light irradiation was followed by the measurement of fluorescence intensity of 2-hydroxy terephthalic acid as reported[18,19]. The experiment consists of irradiating a solution of 50 mL of 0.02 mol L^{-1} NaOH containing 3 m*M* terephthalic acid (TA) and 50 mg of catalyst.

The suspension was stirred in the dark for 60 min before visible light (300 W tungsten lamp) illumination. During irradiation process, 2-3 mL of the suspension was taken out at 60 min intervals, filtered and recorded fluorescence spectra using Shimadzu RF-5301PC fluorescence spectrophotometer. It is well known that the photogenerated $OH^{\bullet}$ radicals react with TA to form 2-hydroxy terephthalic acid (TAOH), which shows a characteristic fluorescence band centered at 425 nm. The increase in the fluorescence intensity of TAOH is directly proportional to the concentration of photo-generated $OH^{\bullet}$ radicals. The excitation wavelength was fixed at 320 nm.

Conductivity measurements

The DC conductivity measurements of KAW and HAW, were recorded in the temperature range 323–623 K by conventional two probe method on the sintered pellets (10 mm in dia.) coated with silver paint. A Keithley electrometer 6485C was used to measure the current.

Results and Discussion

Parent KAW and HAW are prepared by gel burning and ion exchange methods respectively. Fig. 1 shows room temperature XRD patterns of parent (KAW) and proton substituted material, HAW. The *d*-lines of both samples are free from impurities and the powder pattern of HAW is comparable with that KAW[10]. To ascertain the substitution of K^+ by H^+, the powder pattern of HAW was plotted in an expanded scale. All the *d*-lines of HAW have shown a systematic shift towards lower 2θ values. The *d*-lines of HAW present in the 2θ range of 28-32^0 are shown in Fig. S1 (Supplementary Data). The similarity in powder pattern of HAW with that of KAW shows that the lattice is unchanged upon the substitution of K^+ by H^+. Further, the powder XRD result of byproduct is consistent with the powder pattern of KCl (JCPDF: 89-3619) (Fig. S1). Thus, the formation of KCl as byproduct and change in color of sample (Fig. 1, inset) supports the exchange of K^+ by H^+ ions (inset of Fig. 1a). The complete replacement of potassium by H^+ in KAW lattice is also substantiated by recording their energy dispersive spectra (EDS) (Supplementary Data, Fig. S2). The absence of K peaks in EDS of HAW indicates the complete exchange of K^+ by H^+ ions. Hence, the molecular formulas of HAW can be written as $HAl_{0.33}W_{1.67}O_6\ xH_2O$.

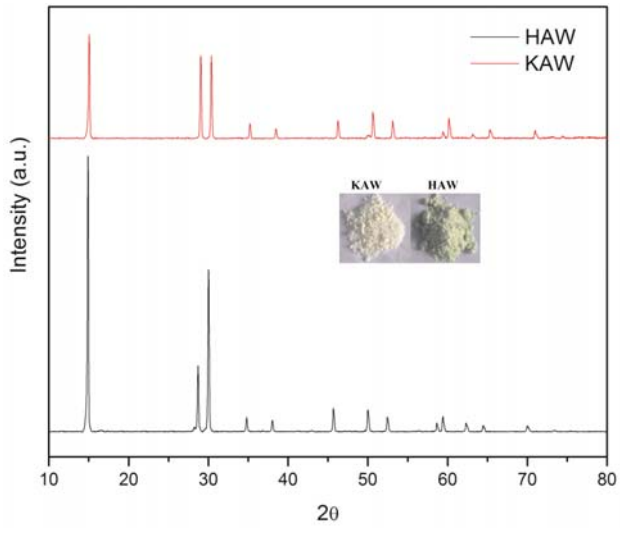

Fig. 1—Powder XRD patterns of KAW and HAW.

Generally, defect pyrochlores have affinity of absorbing moisture from surroundings. These oxides with small A^+ ion (i.e. H^+, Li^+, Na^+, etc.) are all hydrated at room temperature[2,20] and have larger unit cell volume. Thus, at room temperature, the defect pyrochlores can be represented by a general formula $AB_2O_6{\cdot}xH_2O$ (x = amount of absorbed water). This absorbed water can influence the ionic properties of these oxides. The unit cell parameters of HAW are refined by least square fitting the powder data using POWD software. It was found that HAW was crystallized into a cubic lattice with space group $Fd\bar{3}m$. The unit cell parameter and lattice volume of HAW are 10.23 Å and 1070 Å^3 respectively which are comparable with parent KAW[10] (for KAW, a = 10.15 Å and V = 1047 Å^3). The unit cell parameters of HAW marginally increased compared to that of KAW. As the ionic radius of H^+ is lower than K^+, replacement of K^+ by H^+ is expected to shrink the unit cell. But the observed expansion of lattice volume indicates that in addition to H^+, solvent water molecules might have entered into the defect pyrochlore lattice. The presence of water in HAW was confirmed from thermogravimetric analysis (TGA). As shown in Fig. S3 (Supplementary Data), the weight loss of HAW up to the 600 °C may be due to the absorbed water. The weight loss is found to be 4.2%. The weight loss above 600°C is negligible indicating the stability of anhydrous protonated KAW.

The Raman spectrum of HAW is shown in Fig. S4 (Supplementary Data). It is noted that, the Raman

spectral features of HAW are comparable with that of KAW with the exception of slight shift in position and intensity of their bands[10]. This shift may be due to the proton substitution within the host framework. Numerous conclusions on proton position in different defect pyrochlore materials have been reported, although the results seem to be contentious[21-23]. It is also reported that the protonated defect pyrochlore oxides are known to have three types of protonic species, (i) hydroxyl groups (B-OH) close to the $[B_2O_6^{2-}]$ framework, (ii) water molecules hydrogen-bonded to framework hydroxyls, and (iii) H_3O^+ ions hydrogen-bonded to oxygen atoms of the inter cavity window[23]. The ^{1}H NMR and FT-IR measurements are used to identify the presence of different protonic species such as OH^-, H_2O and H_3O^+ in defect pyrochlore structure of HAW. These species can be distinguished by ^{1}H MAS NMR on the basis of their characteristic chemical shift values. The ^{1}H MAS NMR of HAW shows three signals in the range 4 - 8.9 ppm (Fig. 2a). It is reported that the chemical shifts for water of crystallization and hydroxyl protons fall in the region of 4-8 ppm and that of H_3O^+, in the range of 10.5-12 ppm[24,25]. Based on the above affirmation, the three signals observed for HAW in the region 4-8.9 ppm can be attributed to the protons of H_2O and OH^-. The absence of ^{1}H MAS NMR signals in 10.5-12 ppm range implying the lack of free H_3O^+ ions in HAW lattice. These results can be further supported by FT-IR results. Fig. 2b shows the ^{27}Al MAS NMR spectrum of HAW. McKenzie and Smith have reported that chemical shift values for ^{27}Al are very sensitive to its coordination number.

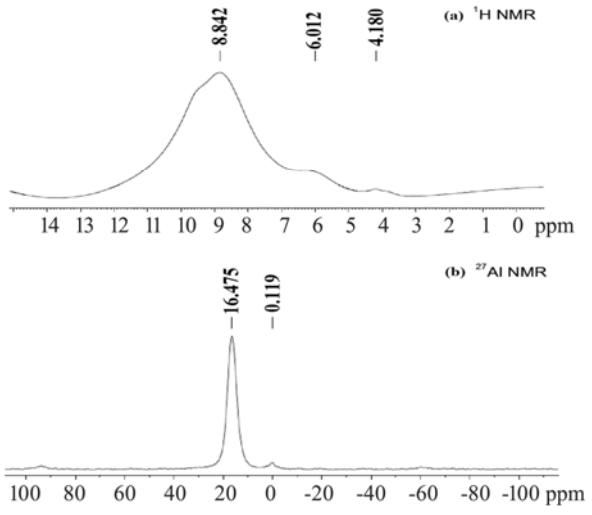

Fig. 2— (a) ^{1}H and (b) ^{27}Al NMR of HAW.

The chemical shift values for ^{27}Al in AlO_6 and AlO_4 sites were found to be in the -5 to 15 ppm and 60-90 ppm, respectively[26]. In the present investigation the signals appeared at -0.119 and 16.475 δ ppm confirms the presence of AlO_6 octahedra in HAW structure. Thus, it can be concluded that proton substituted into the KAW lattice has not altered the local environment of AlO_6 octahedra of the host lattice.

FT-IR spectra of KAW and HAW in the region 400–4000 cm^{-1} is shown in Fig. S5 (Supplementary Data). FT-IR spectrum of HAW shows characteristic vibrational bands, similar to that of KAW along with two additional bands in the 1150-1200 cm^{-1} and 1590-1610 cm^{-1} range. These new bands observed in HAW are due to presence of protonic species in the form of H_2O and OH groups. The sharp absorption band around 1605 cm^{-1} is assigned to bending modes of water[4]. In addition, the absorption band in the 1150-1200 cm^{-1} range is attributed to the Al/W-OH bending mode[27-29]. Thus, it can be concluded that HAW have both the hydroxyl (OH^-) and hydrate (H_2O) protons.

The optical properties of proton exchanged KAW were examined by UV-visible diffuse reflectance spectroscopy. The absorbance versus wavelength plots of KAW and HAW are shown in Fig. S6 (Supplementary Data). It is observed that the absorption edges of protonated samples has been red shifted about 80 nm compared to its parent material. The corresponding bandgap energy (E_g) of HAW is estimated to be 2.41 eV, from a plot of the Kubelka-Munk (KM = $(Kh\nu)^{1/2}$) vs hν) (Fig. S6). Thus, the insertion of proton into KAW lattice has changed its optical properties. It is well known that the optical properties of a material influence the photocatalytic activity considerably. A photocatalytic process is initiated by illumination of light energy equal to or greater than the bandgap energy of catalyst, to create the charge carriers (electron – hole pairs) which are responsible for the generation of reactive hydroxyl and/or superoxide radicals. Therefore, the light absorption capacity of the catalyst plays a significant role in the catalytic process. In addition to light absorption capacity of the catalyst, the efficiency of the catalytic process also depends on the nature of the pollutant, crystallinity of the catalyst, its size, surface area, rate of electron-hole pair generation and recombination etc.

Photocatalytic activity

The visible light photodegradation of methylene blue (MB) and Rhodamine B (RhB) was studied in

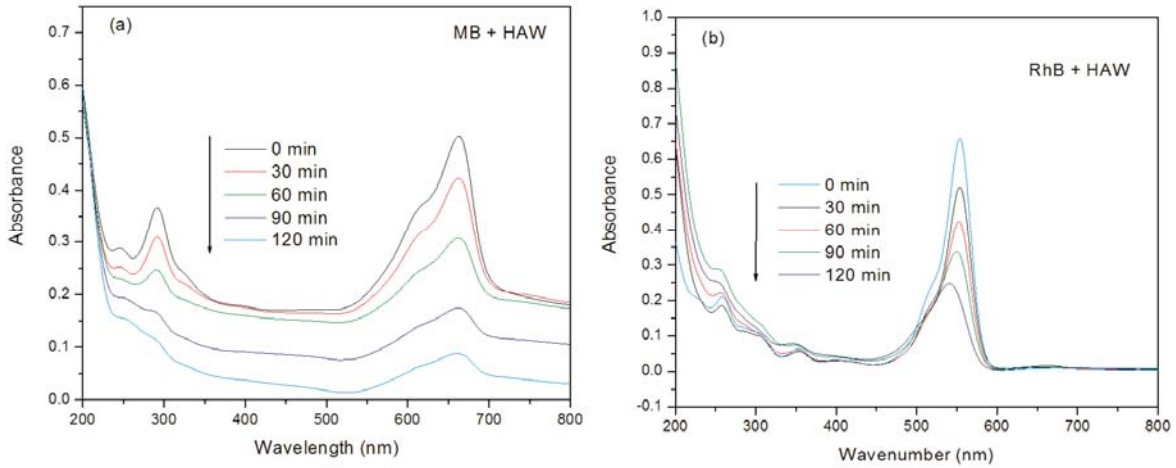

Fig. 3—Temporal changes in the concentration of (a) MB and (b) RhB in the presence of HAW catalyst under the visible light irradiation.

the presence of HAW. The temporal change in MB and RhB absorbance with irradiation time in the presence of HAW is shown in Fig. 3a and 3b respectively. It is perceived that, the decolorization of MB and RhB increase with an increase in the irradiation time. The degradation of MB and RhB was found to be 84 and 63% respectively in the presence of HAW at 120 min of irradiation (Fig. 4). The degradation behavior of MB and RhB in the absence of HAW is also shown in Fig. S7 (Supplementary Data). Under the similar experimental conditions, KAW has shown 67% and ≈0% degradation of MB and RhB respectively[10]. Thus, HAW exhibits better photoactivity in visible light against the degradation of MB and RhB. The enhanced photocatalytic activity of HAW may be credited to lower the bandgap energy of HAW leading to an increase in the number of absorbed photons. Photocatalytic activity of HAW was compared with that of earlier reported defect pyrochlores, $KCr_{0.33}W_{1.67}O_6$ (KCW)[30] and $KFe_{0.33}W_{1.67}O_6$ (KFeW)[31]. It is observed that KCW and KFeW degrades, respectively, about 4.87×10^{-7} moles and 1.43×10^{-5} moles of MB in 120 minutes of visible light irradiation, while HAW degrades 8.27×10^{-6} moles MB under identical experimental conditions. Hence, it may be concluded that the degradation of MB in the presence of HAW, KAW, KCW and KFeW follows the order KFeW > HAW > KCW > HCW.

In general, the photocatalytic degradation rate of organic dyes is directly proportional to the probability of the formation of $^{\bullet}$OH radicals on the surface of catalyst and their reaction with the dye molecules[32]. Due to the lower bandgap energy, HAW is expected

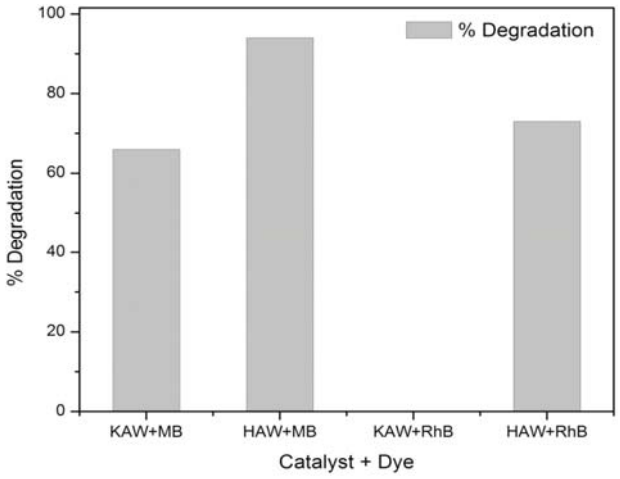

Fig. 4—Photocatalytic degradation of MB and RhB in the presence of KAW and HAW catalysts.

to produce more $^{\bullet}$OH radicals in the photodegradation process compared to KAW. The generation of hydroxyl radicals during the photodegradation in the presence of KAW and HAW has been determined experimentally using TA as probe. As discussed in experimental section, the photogenerated $^{\bullet}$OH radicals react with TA to give 2-hydroxyterephthalic acid (TAOH) which has a characteristic fluorescence signal at 425 nm. It was observed that the fluorescence intensity of TA solution in the presence of HAW and KAW increased at regular time intervals of visible light irradiation. The higher emission intensity of TA over HAW catalyst compared to KAW was observed (Fig. 5). It indicates that HAW produces more $^{\bullet}$OH radicals (or formation of TAOH) due to its lower bandgap energy/higher light absorption compared to KAW.

The kinetics of MB and RhB degradation in the presence of HAW was studied The kinetic plot of $\ln(C/C_0)$ versus time for MB and RhB degradation in the presence of HAW gave a straight line suggesting a pseudo first order kinetics (Langmuir-Hinshelwood model[33]) (Supplementary data, Fig. S8). The equation is

$$\ln (C/C_0) = - kt$$

The rate constants (k) for the reaction are obtained by the slope of the linear line. The half-life time ($t_{1/2}$) calculated from the equation, $t_{1/2} = \ln 2/k$. The obtained kinetic parameters are given in Table 1.

Conductivity studies

As discussed earlier, absorbed water influences the ionic properties of oxide materials. Attempts to explain the role of H_3O^+ ions and water of crystallization in conduction mechanism of protonated oxides has been described[5,34]. Further, the metal (M) ions present in octahedral coordination also influence the electrical properties of the pyrochlores. It is noted that high polarizable B-O-B linkages favour the fast A^+ ion mobility in the defect pyrochlore lattice[3,35,36]. S.V. Bhat et al reported that in defect pyrochlore compounds, the conduction occurs via the exchange of protons of H_2O molecules and OH^- groups[37].

The DC conductivity of KAW and H^+ doped $KAl_{0.33}W_{1.67}O_6$ was studied. The variation in DC conductivity with temperature was shown in Fig. 6.

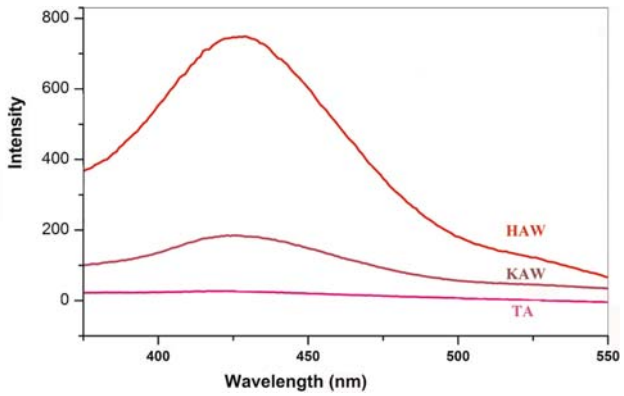

Fig. 5—Fluorescence spectra of 3 m*M* TA ($\lambda_{excitation}$ = 320 nm) in the absence and presence of KAW and HAW at 120 min of visible-light irradiation.

Table 1—Rate constants (k) and half-life time ($t_{1/2}$) of photocatalysts in the first order catalytic degradation of MB and RhB

Catalyst	k (min^{-1})	$t_{1/2}$ (min)	Corr. coeff. (R^2)
MB+HAW	0.014	49.5	0.92
RhB+HAW	0.008	86.6	0.98

The conductivity of parent compound was found to increase linearly with the increase in temperature. However, the conductivity of HAW shows slight decrease up to 120 °C and subsequently increases with increase in temperature. The decrease in conductivity at low temperature region corresponds to dehydration of the adsorbed water, which results a decrease in the movement of ions in the lattice. The variation in conductivity of HAW in the temperature range 323 - 623 K follows Arrhenius equation given by

$$\sigma_{dc}T = \sigma_0 \exp\left(-\frac{E_a}{k_B T}\right)$$

The activation energy (E_a) for conduction and pre-exponential factor (σ_0) are regarded as approximately temperature independent. The experimental data were fitted to the above equation. The activation energies for KAW and HAW are calculated from the slope of the linear fits in the Arrhenius plots and listed in Table 2 along with their dc conductivity at 623 K. A comparison of the conductivity of KAW and HAW shows the following features: (a) at any given temperature, the conductivity of these samples follows the order HAW > KAW, and (b) HAW

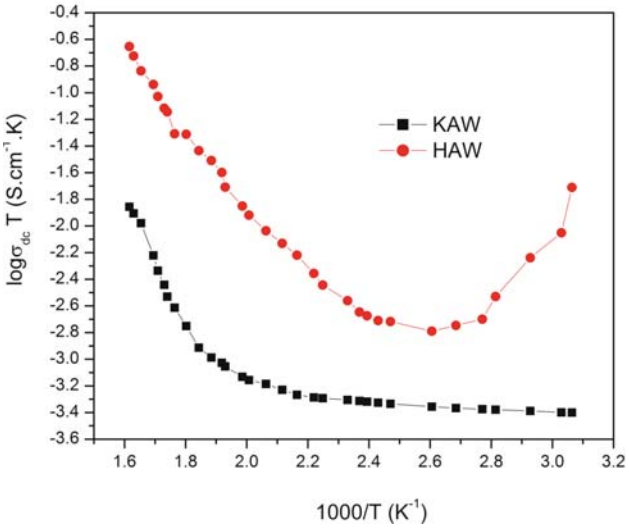

Fig. 6—Arrhenius plots of the ionic conductivity for the KAW and HAW.

Table 2—DC conductivity (at 623 K) and activation energies of KAW and HAW

Parameter	KAW	HAW
DC conductivity at 623 K (S cm^{-1})	2.28×10^{-5}	3.66×10^{-4}
E_a (eV)	0.975	0.620

exhibits 15-fold increase in conductivity compared to that of KAW. The higher conductivity of HAW than KAW can be endorsed to the exchange of protons of H_2O molecules and OH^- groups through interconnecting channels of their lattice.

Pb^{2+} removal using KAW

The procedure for the Pb^{2+} removal using KAW is discussed in the experimental section. The powder XRD pattern of PbKAW is shown in Fig. S9 (Supplementary Data). The powder patterns of both the samples are similar, indicating that the KAW has retained the same structure even after the exchange of Pb^{2+} ions in $Pb(NO_3)_2$ solution. The SEM image of Pb^{2+} ion doped KAW is shown in Fig. 7. The morphology of PbKAW was similar to that of parent KAW[10]. The presence of Pb peak in EDS confirms the exchange of K^+ ions by Pb^{2+} ions (Fig. 7). The EDS data of PbKAW shows that about 38% of K^+ ions are replaced by Pb^{2+} ions. This result was further substantiated from the AAS measurements made on the filtrate of lead nitrate solution after the ion exchange process. The AAS results have shown that about 40% of K^+ ions were exchanged by Pb^{2+} ions. Hence, KAW can be used for removal of heavy metal ion, Pb^{2+}, from aqueous solutions.

In general, the ion exchange process can be influenced by the factors such as (i) the type and/or properties of the medium in which the ions interact with, (ii) size of the ion, (iii) the properties of the chemical compound and (iv) pH of the solution. Han et al. carried out ion exchange experiment for removal of Pb^{2+} using $KNbWO_6$ H_2O at a pH ranging from 2.0 to 5.0, under magnetic stirring at room temperature for 30 h. The ion exchange efficiency was found to increase from 41.0% to 65.4% as the pH value varies from 2.0 to 5.0 and a high pH value is favorable for Pb^{2+} exchange[14]. Therefore, Pb^{2+} exchange efficiency can be improved by changing the experimental conditions such as reaction time, pH and concentration of aqueous $Pb(NO_3)_3$ solution.

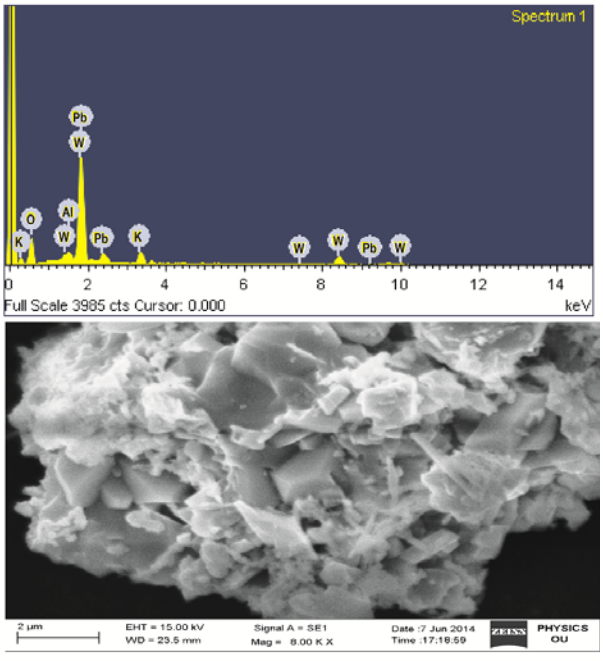

Fig. 7—SEM-EDS of PbKAW.

Conclusions

The protonated KAW was prepared by facile ion exchange method using 5M concentrated HCl at room temperature. HAW was found to be crystallized in cubic lattice with $Fd\bar{3}m$ space group. The proton substitution into KAW was confirmed by (i) shift in *d*-spacings (ii) color of the sample (iii) FT-IR analysis (iv) EDS study and (v) XRD of byproduct, KCl, in ion exchange process. The absorbed water content in protonated oxide was evaluated by thermogravimetric analysis. The band gap energy of HAW, deduced from DRS, was 2.41 eV. MB and RhB degraded to the extent of 84 and 63 % in the presence of the HAW. The higher photocatalytic activity of HAW than that of KAW may be credited to its lower the bandgap energy. The formation of hydroxyl radicals in photocatalytic degradation process was confirmed by TA experiment. The proton conductivity of KAW and HAW was studied in the range 323-623K. HAW exhibits 15-fold increase in conductivity compared to that of KAW. The activation energy of both the materials was calculated by linear fit. KAW can be used for removal of heavy metal ion, Pb^{2+}, from aqueous solutions.

Supplementary Data

Supplementary Data associated with this article, viz., Figs S1-S9, are available in the electronic form at http://www.niscair.res.in/jinfo/ijca/IJCA_56A(03)270-277_SupplData.pdf.

Acknowledgement

The authors gratefully acknowledge the Department of Science & Technology (DST), New Delhi, India, under FIST and University Grants Commission (UGC), New Delhi under UPE-FAR schemes for financial assistance.

References

1 Goodenough J B, Hong H Y P & Kafalas J A, *Mater Res Bull*, 11 (1976) 203.
2 Subramanian M A, Aravamudan G & Subba Rao G V, *Prog Solid State Chem*, 15 (1983) 55.
3 Turrillas X, Delabouglise G, Joubert J G, Fournier T & Muller J, *Solid State Ionics*, 17 **(**1985) 169.
4 Ravinder Guje, Reddy J R, Sudhakar Reddy CH, Sreenu K, Ravi G & Vithal M, *Adv Mater Lett*, 7 (2016) 536.
5 Catti M, Mari C M, Cazzanelli E & Mariotto G, *Solid State Ionics*, 40/41 (1990) 900.
6 Mangamma G & Shahi K, *Solid State Ionics*, 76 (1995) 337.
7 Nader Binesh, Vasudeva Bhatb & Bhat S V, *Solid State Ionics*, 86-88 (1996) 665.
8 Hinrichs R, Tomandl G & da Jornada J A H, *Solid State Ionics*, 77 (1995) 257.
9 Riviere M, Fourquet J L, Grins J & Nygren, *Mater Res Bull*, 23 (1988) 965.
10 Ravi G, Veldurthi N K, Suresh P, Radha V, Someshwar P, Raju Reddy J & Vithal M, *Photochem Photobiol*, 89 (2013) 824.
11 Ravi G, SravanKumar K, Ravinder G, Sreenu K, Prasad G, & Vithal M, *J Solid State Chem*, 233 (2016) 342.
12 Ravi G, Shrujana P, Palla S, Reddy J R, Guje R, Velchuri R & Vithal M, *Micro Nano Lett*, 9 (2014) 11.
13 Uma S, Singh J & Thakral V, *Inorg Chem*, 48 (2009) 11624.
14 Han Y N, Jiao S, Xu M, Pang G & Feng S, *RSC Adv*, 4 (2014) 14357.
15 Moller T, Clearfield A & Harjula R, *Micropor Mesopor Mater*, 54 (2002) 187.
16 Abe M & Itoh T, *J Inorg Nucl Chem*, 42 (1980) 1641.
17 Zarbin A J G, Alves O L, Amarilla J M, Rojas R M & Rojo J M, *Chem Mater*, 11 (1999) 1652.
18 Ishibashi K, Fujishima A, Watanabe T & Hashimoto K, *Electrochem Commun*, 2 (2000**)** 207.
19 Ravinder Guje, Ravi Gundeboina, Ramaswamy Kadari, Sreenu K, Sudhakar Reddy CH, Malathi M, Radha Velchuri & Vithal M, *Indian J Chemi*, 55A (2016) 1174.
20 Tanika Kar & Choudhary R N P, *Mater Sci Eng*, B90 (2002) 224.
21 Groult D, Pannetier J & Raveau B, *J Solid State Chem*, 41 (1982) 277.
22 Dickens P G & Weller M T, *Solid State Commun*, 59 (1986) 569.
23 Alonso J A & X Turrillas, *Dalton Trans*, (5) (2005) 865.
24 Bhat S V, Nader Binesh & Bhat V, *Chem Phys Lett*, 231 (1994**)** 487.
25 Ratcliffe C I, Ripmeester J A & Tse J S, *Chem Phys Lett*, 120 (1985**)** 427.
26 Vyalikh A, Massiot D & Scheler U, *Solid State Nucl Magn Reson*, 36 (2009) 19.
27 Vasudeva Bhat & Gopalakrishnan J J, *Solid State Chem*, 63 (1986) 278.
28 Nakamoto K (2nd Eds), *Infrared Spectra of Inorganic and Coordination Compounds*, (Wiley, USA) 1970.
29 Nyquist R A & Kagel R O *Infrared Spectra of Inorganic Compounds*, (Academic Press, USA) 1971.
30 Ravi G, Naveen Kumar V, Muvva D P, Muniratnam N R, Prasad G & Vithal M, *J Nanopart Res*, 15 (2013) 1939.
31 Ravi G, Suresh P, Naveen Kumar V, Reddy J R, Hari Padmasri A, & Vithal M, *Int J Hydrogen Energy*, 39 (2014) 15352.
32 Luan J, Zhao W, Feng J, Cai H, Zheng Z, Pan B, Wu X, Zou Z & Li Y, *J Hazard Mater,* 164 (2009**)** 781.
33 Liu Y, Chen X, Li J & Burda C*, Chemosphere* 61 (2005) 11.
34 Mari C M, Bonino F, Catti M, Pasinetti R & Pizzini S, *Solid State Ionics Diffus React*, 18/19 (1986**)** 1013.
35 Sleight A W, Gulley J E & Berzins T, *Adv Chem Series*, 163 (1977**)** 195.
36 Guje R, Ravi G, Suresh Palla, Nageshwar Rao K & Vithal, M, *Mater Sci Eng B*, 198 (2015**)** 1.
37 Bhat S V, Nader Binesh & Bhat V, *Chem Phys Lett*, 231 (1994**)** 487.